Energy Conversion and Management: X 12 (2021) 100112

Contents lists available at ScienceDirect

Energy Conversion and Management: X

journal homepage: www.sciencedirect.com/journal/energy-conversion-and-management-x

Using concentrating-solar-power plants as economic carbon-free capacity resources

Kenjiro Yagi [a], Ramteen Sioshansi [a,b,*], Paul Denholm [c]

[a] Department of Integrated Systems Engineering, The Ohio State University, 1971 Neil Avenue, Columbus, OH 43210-1271, United States
[b] Department of Electrical and Computer Engineering, The Ohio State University, 2015 Neil Avenue, Columbus, Ohio 43210-1272, United States
[c] Strategic Energy Analysis Center, National Renewable Energy Laboratory, 15013 Denver West Parkway, Golden, CO 80401-3305, United States

ARTICLE INFO

Keywords:
Concentrating solar power
Thermal energy storage
Peaking generation
Capacity value

ABSTRACT

Deep decarbonization of electricity systems raises concerns about the need for generating capacity that can maintain reliable energy supply. Given this concern, we explore the ability of concentrating-solar-power plants with thermal energy storage to provide a carbon-free source of such capacity. We develop an approach to assessing the capacity contribution of concentrating-solar-power plants that considers future systems. Such considerations are important, because of potential differences in net-load patterns compared to today (*e.g.*, due to higher renewable-energy penetrations). Using historical data spanning an 18-year period, we demonstrate that concentrating-solar-power plants with thermal energy storage can provide this necessary capacity with little impact on their financial viability. We examine the impact of myopic decisions and imperfect foresight of future system conditions on the operation of concentrating-solar-power plants and the resultant impact on their capacity contributions. We find that imperfect foresight can have limited impacts on such a use of concentrating-solar-power plants, so long as proper forecasting techniques are developed and used. Overall, our work shows that concentrating-solar-power plants with thermal energy storage may have a role to play in delivering reliable electricity supply in a decarbonized energy system.

1. Introduction

Due to learning and other effects, concentrating-solar-power (CSP) plants are seeing technology improvements [1]. CSP plants can incorporate high-efficiency thermal energy storage (TES), which allows the plants to become partially dispatchable sources of carbon-free electricity [2]. Denholm et al. [3] provide a comprehensive discussion of the role of energy storage in power systems with high penetrations of renewable energy. Sioshansi et al. [4] survey some of the unique challenges in modeling energy storage, including energy storage that is coupled with renewable-energy sources. A CSP plant with TES has the potential to have a high capacity value, meaning that it can contribute to the power system serving load reliably [5]. This potential is of value as carbon constraints limit the ability of power systems to rely on fossil-fueled generation [6]. Madaeni et al. [7] examine the capacity value of CSP plants without TES. Madaeni et al. [8] expand this analysis to show the added capacity-value benefits of incorporating TES into CSP plants. There are additional benefits to incorporating TES into CSP, beyond capacity value [9]. These analyses [5,7–9] are based, however, on examining supply and demand patterns of current power systems. Indeed, the high capacity values of CSP plants with TES are driven by the current co-incident peaks in electricity demand and solar availability (*e.g.*, during hot summer afternoons) in many power systems.

Thus, most extant studies of the capacity value of CSP plants neglect the impact that increasing penetrations of variable renewable-energy resources may have on future net-load patterns. The proliferation of renewable energy can result in net-load patterns that look significantly different than today's demands, which may yield significant mismatches between peaks in net load and solar availability. These load changes may require 'smarter' power systems that can deliver capacity reliably during periods that are of less concern today. Yagi et al. [10] conduct a more forward-looking analysis of the capacity value of CSP plants with TES. Using 18 years of historical data for a variety of locations in the southwestern United States of America (US), they demonstrate that a properly sized CSP plant with TES can maintain reliable energy supply during the eight highest-load hours of almost all of the days of the year

* Corresponding author at: Department of Integrated Systems Engineering, The Ohio State University, 1971 Neil Avenue, Columbus, OH 43210-1271, United States.
E-mail addresses: yagi.7@buckeyelink.osu.edu (K. Yagi), sioshansi.1@osu.edu (R. Sioshansi), paul.denholm@nrel.gov (P. Denholm).

https://doi.org/10.1016/j.ecmx.2021.100112

Available online 5 October 2021

[10]. Thus, Yagi et al. [10] show that CSP plants with TES can play a major role ensuring reliable energy supply in decarbonized electricity systems.

An important limitation of much of the extant literature regarding the capacity value of CSP plants [5,7–10] is that they assume that the CSP plants are operated solely to serve capacity needs. Thus, for the most part they neglect the desire of a CSP-plant owner to maximize the value of energy that the plant produces. Maximizing CSP-plant profit is important to ensure that the plant is a *cost-effective* and *economic* source of reliable energy supply. Another limitation of the existing literature is that much of it neglects the impact of uncertainty on operating CSP plants. Uncertainty can impact the reliability benefits of a CSP plant, because energy that is stored in TES may be depleted before it is needed to meet an unanticipated load peak.

This paper provides a more comprehensive analysis of the reliability benefits of CSP plants with TES and addresses these key limitations of the existing literature. Specifically, we examine the operation of a CSP plant with TES from the perspective of a profit-motivated plant owner. The plant is assumed to be operated to maximize the profit that is earned from its selling energy, while meeting system-reliability targets. Specifically, we set a target that the CSP plant have sufficient energy available to operate at its rated capacity during the eight highest-load hours of a set number of days of the year. The target does not require that the plant be operating at its nameplate capacity during the highest-load hours—only that it has sufficient energy available to operate at its nameplate capacity if system conditions warrant its doing so. We apply the target to the days with the highest peak loads (*e.g.*, if the target is applied to thirty days, the thirty days with the highest peak loads are chosen). We set the reliability target in this manner to determine whether the operational flexibility that TES engenders allows a CSP plant to serve power-system-reliability needs in the future when net-load patterns may have non-trivial differences compared to today. If a CSP plant can provide energy during the eight highest-load hours of a day, one may infer that it has sufficient operational flexibility to serve peaks under future load patterns.

We conduct our analysis under three sets of operational assumptions. First, we assume that the CSP-plant operator has perfect foresight of system conditions (*i.e.*, hours to which the reliability target applies, prices, and weather) and optimizes CSP-plant operations over the full year. Thus, this set of assumptions yields an ideal benchmark, wherein neither forecast errors nor myopic decisions reduce the profit or reliability contribution of the CSP plant. We show that under these ideal assumptions, CSP plants can, on average, cover at least 98.4% of peak-load requirements during the full year.

Our second set of assumptions introduces myopic decision making but retains perfect foresight. CSP-plant operations are assumed in this case to be optimized one hour at a time in a rolling-horizon fashion, using a 24-h optimization horizon. Using a 24-h optimization horizon is a heuristic approach to obtaining decisions that are somewhat forward-looking [11]. Specifically, the 24-h optimization horizon allows the use of TES to shift energy within a one-day period, but does not allow explicit shifting of energy beyond one day [12]. Real plant operators may not use TES to shift energy multiple days into the future. This set of assumptions allows us to understand the impact of myopic decisions with limited foresight and yields decisions that are closer to real-world operation compared to the ideal benchmark. We show that myopic decisions can reduce the ability of the CSP plant to cover the peak-load requirement by two or three percentage points relative to the ideal benchmark. We show also that operating a CSP plant to meet the peak-load requirement reduces its profit by at most 1.2% compared to a case of operating the plant solely to maximize profit. These findings imply that the operational flexibility of CSP plants makes them a cost-effective source of supply reliability to decarbonized power systems.

Our final set of assumptions relaxes perfect foresight and optimizes plant operations myopically using persistence or moving-average forecasts. We use relatively simple forecasting techniques. Thus, this set of assumptions yields a bounding worst case of how uncertainty can impact CSP plants serving as capacity resources. Actual CSP-plant operators may have access to higher-fidelity forecasting techniques, which could improve upon our results. We demonstrate that using these simple forecasting approaches reduce the reliability benefits and operating profits of CSP plants by less than 11% and 16%, respectively, relative to having perfect foresight. Overall, our results show that even with uncertainty CSP plants can serve as economic sources of power-system reliability. However, improved forecasting will be critical for such use of CSP plants, which is an important area of research for improving the competitiveness of this technology.

Our work makes four key contributions to the existing literature. First, we examine the capacity value of a profit-motivated CSP-plant operator. This can be contrasted with other works [5,7–10] that assume that CSP plants are operated by a central planner solely based on their capacity contributions. Second, we conduct a detailed examination of how myopic decisions impact the capacity value of a CSP plant. Third, we show that the operational flexibility that is engendered by TES allows a CSP plant to have a high capacity value without undue impact on its profitability. Fourth, we examine what uncertain data have the greatest impact on the use of a CSP plant as a capacity resource.

The remainder of this paper is organized as follows. Section 2 discusses our assumptions regarding the CSP technology that is modeled, including the key sizing parameters of solar multiple (SM) and TES capacity. Section 3 describes our methodology. Sections 4 and 5 summarize, respectively, the data underlying and implementation of our case study. Section 6 summarizes case-study results. Section 7 concludes.

2. CSP assumptions

We focus our analysis on tower-type CSP plants. Other CSP-plant types, such as parabolic-trough systems [13], are excluded from our analysis. Baharoon et al. [14] provide a history of the development of CSP technology. Mehos et al. [15] discuss technology, performance, and dispatchability advances of the technology. Tower-type CSP plants consist of an array, which typically is referred to as a solar field, of heliostats. The heliostats reflect the direct normal (beam) component of solar irradiance towards a central receiver. The concentrated solar energy heats a working fluid, *i.e.*, a molten salt. The working fluid goes to the TES system, which consists of an insulated tank, and can be directed towards the powerblock, which consists of a salt-to-water heat exchanger and a conventional steam-turbine generator.

The size of the powerblock in a CSP plant is expressed typically by its rated capacity. Powerblock capacity can be given as the maximum thermal power that can be input (measured in MW-t) or maximum electric output (measured in MW-e). The size of a solar field is measured often by its SM. A solar field with an SM of 1.0 is sized to produce enough energy to drive the powerblock at its rated output under design weather conditions. Because these design conditions occur rarely, an SM greater than 1.0 is typical in modern CSP plants. The energy-storage capacity of a TES system is measured typically by the number of consecutive hours that the plant can operate at full output using only energy from a fully charged TES system. We focus on two solar-field and TES configurations—plants with an SM of 2.0 and six hours of TES and plants with an SM of 3.0 and 12 h of TES. Based on recent CSP-deployment trends, we assume a powerblock with a rated gross output capacity of 222 MW-e, which corresponds to a rated input capacity of 538 MW-t. The net output of a CSP plant is reduced due to parasitic loads from operating the motors on the heliostats, pumps that circulate the working fluid through the TES and powerblock, and condensers. Six hours of TES corresponds to about 3.23 GWh-t for this plant configuration (*i.e.*, with a 222-MW-e powerblock). Prolonged periods with high solar availability can result in total energy that is collected by the solar field exceeding the energy-storage capacity of TES, in which case excess thermal energy must be curtailed.

3. Methdology

Our analysis consists of a two-step simulation [16]. First, we employ a physical model to determine how much thermal energy the CSP plant's solar field captures during each hour of each year that we analyze. Second, we use an optimization model to determine how the CSP plant is operated during each hour to maximize its profit while aiming to meet its reliability target.

3.1. Solar-Field Model

We simulate the solar field using version 2017.1.17.r1 of System Advisor Model (SAM) [17]. SAM takes as an input hourly weather data and determines the amount of thermal energy that is collected by the receiver in the simulated CSP plant's tower.

3.2. Optimization-model overview

We use a two-stage stochastic optimization model, which is adapted from the work of Sioshansi and Denholm [18], to determine the hourly operation of the CSP plant and its TES. Depending on operating constraints, thermal energy that is collected by the CSP plant's receiver can be fed immediately into the plant's powerblock to produce electricity or can be stored in the TES. Stored energy in the TES can be used to supplement thermal energy from the receiver to drive the powerblock.

3.3. Optimization-model notation

We define the following sets, indices, parameters, and functions that are used in formulating the optimization model.

C	variable generation cost of CSP plant [$/MWh-e]
$E^{\mathrm{SF}}_{\omega,t}$	thermal energy that is collected under scenario ω during hour t by the receiver [MWh-t]
E^{SU}	energy that is consumed to start-up the powerblock [MWh-t]
$F_{\omega,t}(\cdot,\cdot)$	hour-t powerblock heat-rate function under scenario ω [MWh-e]
$H^{\mathrm{RD}}_{\omega,t}$	number of consecutive hours that reliability target requires CSP plant to operate starting from hour t under scenario ω [h]
K	penalty for not meeting reliability target [$/MWh-t]
$M_{\omega,t}$	hour-t electricity price under scenario ω [$/MWh-e]
$P^{\mathrm{PB}}_{\omega,t}(\cdot,\cdot)$	hour-t powerblock-parasitic-load function under scenario ω [MWh-e]
$P^{\mathrm{SF}}_{\omega,t}$	hour-t solar-field parasitic load under scenario ω [MWh-e]
t	time index
$T = \{t_{\mathrm{st}},\ldots,t_{\mathrm{en}}\}$	ordered set of hourly time periods in the optimization horizon from t_{st} to t_{en}
T^{TG}_{ω}	set of target hours under scenario ω
$\Theta^{\max}$	maximum thermal-energy input to the powerblock during an hour that it is online [MWh-t]
$\Theta^{\min}$	minimum thermal-energy input to the powerblock during an hour that it is online [MWh-t]
κ	energy-carrying capacity of the TES system [h]
π_{ω}	probability of scenario ω occurring
Υ	self-discharge rate of TES system [p.u.]
ω	scenario index
Ω	set of scenarios

We model the operation of the CSP plant over an ordered set, T, of hourly time periods and over a set, Ω, of scenarios. Each scenario, $\omega \in \Omega$, corresponds to a possible realization of uncertain system conditions (*e.g.*, energy prices, reliability need of the power system, and weather). T^{TG}_{ω} is the set of hours, under scenario ω, during which the reliability target requires that the CSP plant be able to operate at its nameplate capacity. In our case studies, the target hours are the eight highest-load hours of a predetermined number of days of the year. If the CSP plant has a reliability-related requirement during hour t under scenario ω, $H^{\mathrm{RD}}_{\omega,t}$ indicates the consecutive number of hours that the plant must be able to produce energy starting from hour t. In many cases, the eight highest-load hours of a day occur consecutively. In such a case, $H^{\mathrm{RD}}_{\omega,t}$ equals eight during the first hour of the consecutive block and the values of $H^{\mathrm{RD}}_{\omega,t}$ decrease by one to a value of one for the final hour of the consecutive block. In some instances (*e.g.*, during winter days) the highest-load hours of the day may occur during multiple blocks (*e.g.*, in the early morning and late evening, due to lighting and heating demands). In such a case, the values of $H^{\mathrm{RD}}_{\omega,t}$ indicate the remaining number of consecutive hours during a block of target hours.

Operating the plant's solar field (*e.g.*, rotating the heliostats) imposes a parasitic load of $P^{\mathrm{SF}}_{\omega,t}$ MWh-e during hour t of scenario ω. The powerblock imposes parasitic loads as well, *e.g.*, to circulate thermal fluid. $P^{\mathrm{PB}}_{\omega,t}(\cdot,\cdot)$ gives this parasitic load during hour-t under scenario ω. K is a penalty parameter for not meeting the reliability target. K can be set arbitrarily, so long as it is sufficiently large compared to energy prices to incentivize the CSP plant meeting its reliability target.

We define the following decision variables which are optimized in the model.

$e_{\omega,t}$	supplemental energy that is needed during hour t under scenario ω to meet reliability requirement [MWh-t]
$l_{\omega,t}$	ending hour-t SOE of the TES under scenario ω [MWh-t]
$r_{\omega,t}$	binary variable that equals 1 if the powerblock is started-up during hour t under scenario ω
$u_{\omega,t}$	binary variable that equals 1 if the powerblock is online during hour t under scenario ω
$\theta_{\omega,t}$	hour-t thermal energy that is input under scenario ω to the powerblock [MWh-t]
$\xi^{+}_{\omega,t}$	positive portion of hour-t net electric output of the CSP plant under scenario ω [MWh-e]
$\xi^{-}_{\omega,t}$	negative portion of hour-t net electric output of the CSP plant under scenario ω [MWh-e]

The variable sets, $r_{\omega,t}$ and $u_{\omega,t}$, represent the operating state of the powerblock. The variable set, $\theta_{\omega,t}$, represents thermal energy that is input to the powerblock and the variable sets, $\xi^{+}_{\omega,t}$ and $\xi^{-}_{\omega,t}$, represent the resultant electric output. Electric output can be negative due to the parastic loads. The variable set, $l_{\omega,t}$, is used to track the evolution of the SOE of the TES. The variable set, $e_{\omega,t}$, is used to measure the inability of the plant to meet its reliability target. If the plant has insufficient energy (from its solar field or TES) to operate at its nameplate capacity during a target hour, the corresponding value of $e_{\omega,t}$ measures the energy deficit.

3.4. Optimization-model formulation

The optimization model is formulated as:

$$\max \sum_{\omega\in\Omega,t\in T} \pi_{\omega}\cdot\left[M_{\omega,t}\cdot\left(\xi^{+}_{\omega,t}-\xi^{-}_{\omega,t}\right)-C\cdot\xi^{+}_{\omega,t}-K\cdot e_{\omega,t}\right] \tag{1}$$

$$\text{s.t.}\quad \Theta^{\min}\cdot u_{\omega,t}\leqslant\theta_{\omega,t}\leqslant\Theta^{\max}\cdot u_{\omega,t}-E^{\mathrm{SU}}\cdot r_{\omega,t};\qquad \forall\omega\in\Omega,t\in T; \tag{2}$$

$$\xi^{+}_{\omega,t}-\xi^{-}_{\omega,t}=F_{\omega,t}(\theta_{\omega,t},u_{\omega,t})-P^{\mathrm{PB}}_{\omega,t}(\theta_{\omega,t},u_{\omega,t})-P^{\mathrm{SF}}_{\omega,t};\qquad \forall\omega\in\Omega,t\in T; \tag{3}$$

$$r_{\omega,t}\geqslant u_{\omega,t}-u_{\omega,t-1};\qquad \forall\omega\in\Omega,t\in T; \tag{4}$$

$$r_{\omega,t}\leqslant 1-u_{\omega,t-1};\qquad \forall\omega\in\Omega,t\in T; \tag{5}$$

$$r_{\omega,t}\leqslant u_{\omega,t};\qquad \forall\omega\in\Omega,t\in T; \tag{6}$$

$$l_{\omega,t}\leqslant\Upsilon\cdot l_{\omega,t-1}+E^{\mathrm{SF}}_{\omega,t}+e_{\omega,t}-E^{\mathrm{SU}}\cdot r_{\omega,t}-\theta_{\omega,t};\qquad \forall\omega\in\Omega,t\in T; \tag{7}$$

$$0\leqslant l_{\omega,t}\leqslant\kappa\cdot\Theta^{\max};\qquad \forall\omega\in\Omega,t\in T; \tag{8}$$

$$r_{\omega,t},u_{\omega,t}\in\{0,1\};\qquad \forall\omega\in\Omega,t\in T; \tag{9}$$

$$e_{\omega,t},\xi^{+}_{\omega,t},\xi^{-}_{\omega,t}\geqslant 0;\qquad \forall\omega\in\Omega,t\in T; \tag{10}$$

$$e_{\omega,t_{\mathrm{st}}}=e_{\omega',t_{\mathrm{st}}};\qquad \forall\omega,\omega'\in\Omega; \tag{11}$$

$$l_{\omega,t_{st}} = l_{\omega',t_{st}}; \qquad \forall \omega, \omega' \in \Omega; \tag{12}$$

$$r_{\omega,t_{st}} = r_{\omega',t_{st}}; \qquad \forall \omega, \omega' \in \Omega; \tag{13}$$

$$u_{\omega,t_{st}} = u_{\omega',t_{st}}; \qquad \forall \omega, \omega' \in \Omega; \tag{14}$$

$$\theta_{\omega,t_{st}} = \theta_{\omega',t_{st}}; \qquad \forall \omega, \omega' \in \Omega; \tag{15}$$

$$\xi^{+}_{\omega,t_{st}} = \xi^{+}_{\omega',t_{st}}; \qquad \forall \omega, \omega' \in \Omega; \tag{16}$$

$$\xi^{-}_{\omega,t_{st}} = \xi^{-}_{\omega',t_{st}}; \qquad \forall \omega, \omega' \in \Omega; \tag{17}$$

$$u_{\omega,t} - r_{\omega,t} \geqslant 1; \qquad \forall \omega \in \Omega, t \in T^{TG}_{\omega}; \tag{18}$$

$$\Upsilon \cdot l_{\omega,t-1} + e_{\omega,t} + \sum_{s=t}^{t+H^{RD}_{\omega,t}-1} E^{SF}_{\omega,s} \geqslant E^{SU} \cdot \left(r_{\omega,t} + 1 - u_{\omega,t} \right) + H^{RD}_{\omega,t} \cdot \Theta^{max}; \quad \forall \omega \in \Omega, t \in T^{TG}_{\omega}. \tag{19}$$

Objective function (1) computes expected profit that is earned by the CSP plant, less penalties that are assessed for not meeting the reliability target. The model has two sets of constraints. Constraints (2)–(7) pertain to physical limitations on the operation of the plant. Constraints (18)–(19) enforce the reliability requirements.

Constraints (2) impose lower and upper limits on the amount of thermal energy that can be delivered to the powerblock when it is online. These constraints force zero thermal energy to be delivered when the powerblock is offline. The maximum amount of thermal energy that can be delivered is reduced during hours that the powerblock is started-up. Constraints (3) define the net electricity output of the CSP plant as gross output, which is given by the heat-rate function, less the parasitic loads from the powerblock and solar field. Constraints (4) define the values of the start-up binary variables in terms of intertemporal changes in the values of the online binary variables. Constraints (5) prevent the powerblock from being started-up during hour t if it is online during the previous hour (*i.e.*, the CSP-plant operator could keep the powerblock online as opposed to shutting it down and starting it up immediately thereafter). Constraints (6) require the powerblock to enter an online state when a start-up takes place.

Constraints (7) impose hourly thermal-energy balance and define the ending hourly SOE of the TES. The left-hand side of the hour-t/scenario-ω constraint gives the ending hour-t/scenario-ω SOE of TES. The right-hand side of the constraint gives the total amount of thermal energy that is available to be stored at the end of hour t, which gives the implicit upper bound on $l_{\omega,t}$. This bound is defined as the sum of the amount of energy that is carried from the previous hour, energy that is collected by the solar field, and supplemental energy. From this thermal energy that is available, energy that is used to start-up the powerblock and energy that is fed to the powerblock to produce electricity are subtracted. Constraints (8) impose SOE limits on the TES system. Constraints (9) and (10) impose integrality and non-negativity, respectively, on the appropriate variables.

Constraints (11)–(17) impose uncertainty on the first-stage decisions. This is done by forcing all of the variables during hour t_{st} (when the realization of the scenario that describes future system conditions is unknown) to equal one another across all of the scenarios. Conversely, decisions in subsequent hours are free to vary between the scenarios. This is a standard approach to representing uncertainty in optimization models [19].

Constraints (18) and (19) apply only to target hours and ensure that the reliability requirements are met. Constraints (18) force the CSP plant to be online but not starting-up during target hours. This restriction is imposed because the CSP plant is unable to produce 100% of its rated output during an hour that it is starting-up. Constraints (19) ensure that the plant has sufficient thermal energy available to operate at its rated capacity during the full block of target hours. The right-hand sides of (19) compute the thermal energy that is necessary to maintain plant operations at nameplate capacity during the full block of target hours. These energy requirements are given by the products of the rated thermal-energy capacity of the powerblock, Θ^{max}, and the number of consecutive hours during which the target applies for each hour, H^{RD}_{t}. The left-hand sides of each of these constraints are the total thermal energy that is available to the CSP plant during each hour.

Ramp-rate constraints are excluded from our model. This is because modern CSP plants can ramp over their full operating range in less than one hour [20]. Our model does not consider additional value streams or revenue sources that are provided by the rapid ramping capabilities of CSP plant (*e.g.*, the provision of ancillary services).

4. Case-study data

Our simulations are performed for the 27 locations that are highlighted in Fig. 1. These locations represent a range of sites where CSP plants are technically viable, *i.e.*, there is sufficient direct normal irradiance (DNI) to justify plant construction given the technology's current technical and cost characteristics. The locations that we examine include some at which plants are deployed or in planning stages. Table 1 provides coordinates and annual-average daily DNI for each of the 27 locations.

Our study of each hypothetical plant requires four sets of primary data—system loads (which determine the target hours), electricity prices, assumed design parameters of the plant, and weather data (which determine the plant's real-time operating characteristics).

Fig. 1 indicates the balancing authority from which price and load data are used in simulating the performance of CSP plants at each location (*i.e.*, the operation of each plant is optimized *vis-à-vis* price and load data corresponding to the balancing authority in which it is located). Historical load data for each balancing authority are obtained from Federal Energy Regulatory Commission (FERC) Form 714. Historical electricity-price data are obtained from FERC Form 714 for all balancing authorities except for California Independent System Operator (CAISO) and Electric Reliability Council of Texas (ERCOT). Price data for CAISO and ERCOT are collected from public data repositories on their websites. Table 2 summarizes the years between 1998 and 2015 for which load and price data are available for each balancing authority. We simulate the operations of plants at each location only for years for which we have both load and price data.

Weather data are obtained from National Solar Radiation Database (NSRDB) version 2.0.1. Sengupta et al. [21,22] describe the physical modeling that underlies production of NSRDB and provide a high-level description of the product in a subsequent work [23]. Wilcox [24] provides a guide for its use.

We assume default design parameters, which are given in SAM, for tower-type CSP plants.

5. Case-study implementation

We analyze the performance of the hypothetical CSP plants under three sets of operational assumptions—the ideal benchmark, myopic decision making that assumes perfect foresight or uses day-ahead persistence forecasts, and two-stage stochastic optimization. The input data to and implementation of model (1)–(19) differ between these three sets of assumptions, as detailed in the following subsections.

5.1. Ideal benchmark

The ideal benchmark assumes perfect foresight and no myopic decision making. This case is modeled by solving (1)–(19) for an entire year at once (*i.e.*, $|T| = 8760$ or $|T| = 8784$, depending on whether a given year is a leap year). Because we assume perfect foresight, these

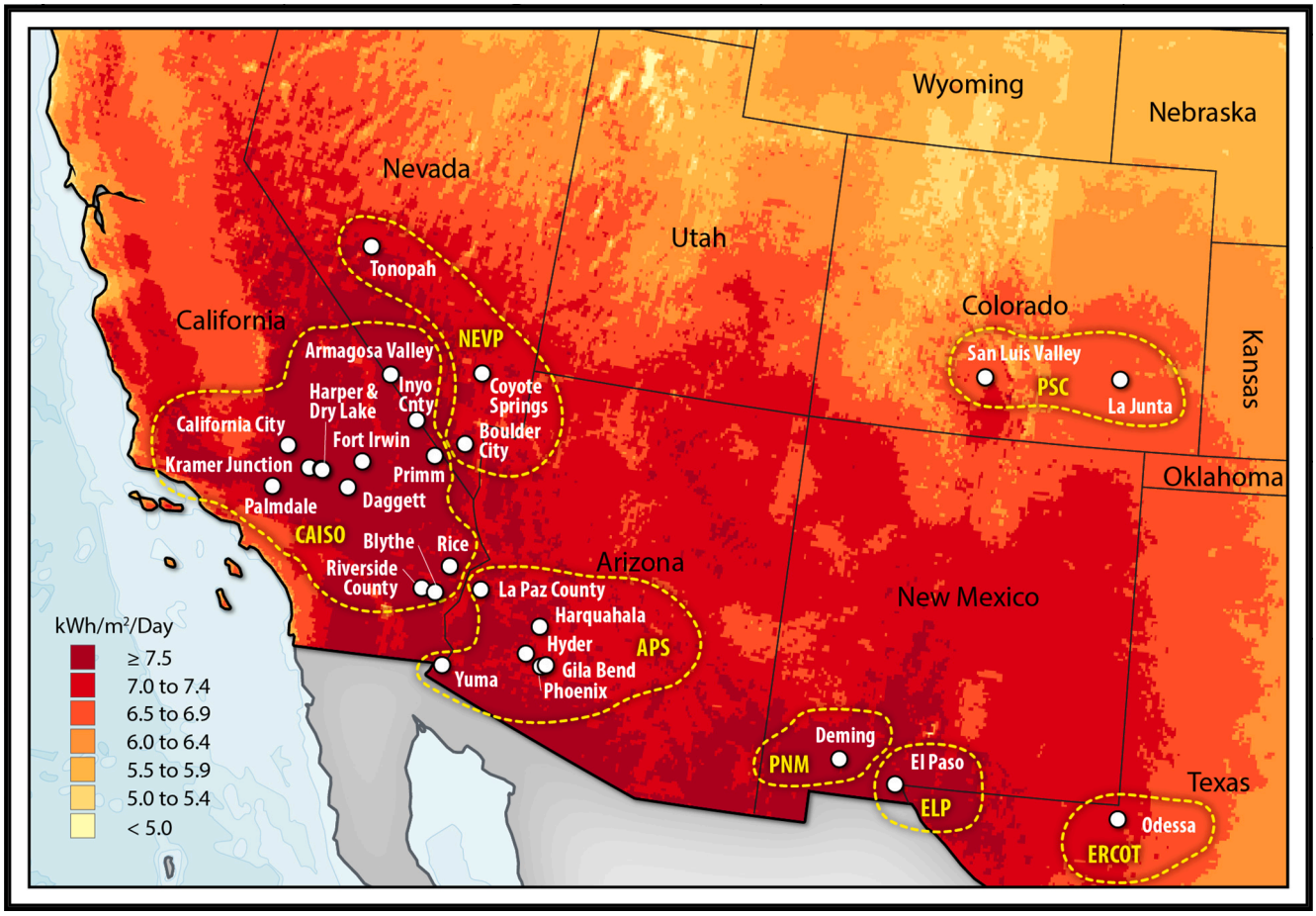

Fig. 1. The 27 locations in the southwestern US that are studied and approximate boundaries of the balancing authorities.

cases are modeled assuming a single scenario (*i.e.*, $|\Omega| = 1$ and $\pi_1 = 1$) and all of the system conditions for the entire year are known with certainty.

The powerblock's heat-rate function is approximated as:

$$F_{1,t}(\theta_{1,t}, u_{1,t}) = \frac{1}{0.412}\eta^{\text{amb}}_{1,t}\cdot(0.4335\cdot\theta_{1,t} - 11.345\cdot u_{1,t}), \forall t \in T;$$

where $\eta^{\text{amb}}_{1,t}$ is a factor that accounts for the effect on powerblock efficiency of hour-t ambient temperature. For all $t \in T$, the value of $\eta^{\text{amb}}_{1,t}$ is estimated based on the work of Wagner et al. [25].

Solar-field parasitics depend solely on energy that is required to operate the motors on the heliostats and have no dependence on how the TES or powerblock are operated. As such, $\forall t \in T$, the value of $P^{\text{SF}}_{1,t}$ is obtained directly from the SAM simulation that is used to determine $E^{\text{SF}}_{1,t}$, $\forall t \in T$. Conversely, powerblock-parasitic load depends on the operation of the plant, which is determined by (1)–(19). The SAM simulation that is used to determine $E^{\text{SF}}_{1,t}, \forall t \in T$ outputs the amount of thermal energy that is fed into the powerblock during each hour, if the plant is operated using SAM's dispatch logic. The thermal energy that is fed into the powerblock is related to the amount of working fluid that must be circulated in the plant and the operation of the plant's condensers. SAM outputs the powerblock's hourly parasitic loads. We fit a linear regression to these outputs (hourly energy input to the powerblock and powerblock-parasitic loads) to estimate $P^{\text{PB}}_{1,t}(\theta_{1,t}, u_{1,t}), \forall t \in T$. Estimating $P^{\text{PB}}_{1,t}(\theta_{1,t}, u_{1,t}), \forall t \in T$ in this way allows us to capture endogenously the effect of dispatch decisions on plant parasitics in (1)–(19).

Model (1)–(19) is formulated using `Python` 2.7 and solved using `Gurobi` version 7.5.1 on a system with two Intel Xeon E5-2697 v4 processors with 18 2.30-GHz cores each and 270 GB of memory. Default solver settings are used, except for the optimality gap, which is set to 2%, and disabling of the aggregator in the presolve step. These settings improve solution times. However, these settings imply that there may be alternative solutions to (1)–(19) that reduce the energy deficit or increase plant profits by at most 2% compared to the solutions that we report. We assume $K = 10000$.

5.2. Myopic decision making

The case of myopic decisions with perfect foresight uses the same input data and scenario structure (*i.e.*, $|\Omega| = 1$ and $\pi_1 = 1$) that are used for the ideal benchmark. The key modeling difference is that plant operations are simulated one hour at a time in a rolling-horizon fashion. Specifically, to determine hour-τ plant operations, an instance of (1)–(19) in which $t_{\text{st}} \leftarrow \tau$ and $t_{\text{en}} \leftarrow \tau + 23$ is solved. This process is repeated starting with $\tau = 1$ (to determine the hour-1 operation of the plant) until $\tau = 8760$ (or $\tau = 8784$ for a leap year). Because (1)–(19) has a 24-h optimization horizon, we can reduce the optimality-gap setting to 0.3% (meaning that the solutions that we report are very near-optimal) with no appreciable computation-time increase.

5.3. Day-ahead persistence forecasts

The cases with day-ahead persistence forecasts are implemented in the same way that the case of myopic decisions is, with one exception. If we assume that a plant operator uses day-ahead persistence forecasts for a random variable, which we will denote generically as ζ, historical data are used to project future values of ζ. More specifically, for each hour of the year, τ, we determine hour-τ plant operations by setting $t_{\text{st}} \leftarrow \tau$ and

Table 1
Coordinates and annual-average DNI of 27 locations in the southwestern US that are studied.

Location Name	Latitude [° N]	Longitude [° W]	Annual-Average Daily DNI [kWh/m^2/day]
Fort Irwin, CA	35.26	116.68	8.22
Kramer Junction, CA	35.01	117.56	8.18
Rice, CA	34.07	114.82	8.13
Harper Dry Lake, CA	35.03	117.35	8.11
Armagosa Valley, NV	36.54	116.52	8.00
Blythe, CA	33.67	114.98	7.97
Harper Dry Lake, CA	35.02	117.33	7.88
California City, CA	35.25	118.01	7.86
Daggett, CA	34.86	116.83	7.83
Primm, NV and CA	35.55	115.46	7.81
Riverside County, CA	33.69	115.22	7.79
Palmdale, CA	34.64	118.11	7.61
Inyo County, CA	35.99	115.90	7.60
Yuma, AZ	32.68	114.62	7.97
La Paz County, AZ	33.83	114.22	7.92
Hyder, AZ	33.06	113.26	7.82
Harquahala, AZ	33.47	113.11	7.82
Gila Bend, AZ	32.95	112.89	7.67
Phoenix, AZ	32.92	112.97	7.57
Boulder City, NV	35.80	114.98	7.60
Tonopah, NV	38.24	117.36	7.52
Coyote Springs, NV	36.82	114.93	7.52
La Junta, CO	37.98	103.54	6.77
San Luis Valley, CO	37.84	105.98	6.76
El Paso, TX	32.00	106.77	8.12
Deming, NM	32.26	107.75	7.94
Odessa, TX	31.80	103.00	7.32

Table 2
Years with available load and price data for each balancing authority.

	Balancing Authority						
Year	APS	CAISO	ELP	ERCOT	NEVP	PNM	PSC
1998	*		*		*	*	*
1999					*	*	*
2000	*	*	*		*	*	*
2001			*		*	*	*
2002	*	*	*		*	*	*
2003	*	*	*		*	*	*
2004	*		*				
2005			*				
2006	*		*		*	*	
2007	*		*		*	*	*
2008	*		*		*	*	*
2009	*		*		*	*	*
2010	*	*	*		*	*	*
2011	*	*	*	*	*	*	*
2012	*	*	*	*	*	*	*
2013	*		*	*	*	*	*
2014	*		*	*	*	*	*
2015	*		*	*	*	*	*

$t_{en} \leftarrow \tau + 23$. We set ζ_τ equal to its true value (based on the historical data that are being used to simulate the operation of a plant at a particular location during a particular year). The values of $\zeta_{\tau+1}, \zeta_{\tau+2}, \ldots, \zeta_{\tau+23}$ are set equal to the values, $\zeta_{\tau-23}, \zeta_{\tau-22}, \ldots, \zeta_{\tau-1}$, which are taken from the previous day.

5.4. Two-stage stochastic optimization

The cases with two-stage stochastic optimization employ the same rolling-horizon approach that we use with persistence forecasts. The key difference is that, for each hour of the year, τ, we determine hour-τ plant operations knowing hour-τ conditions with certainty whereas conditions for the following 23 h are represented using 30 equiprobable scenarios (*i.e.*, $|\Omega| = 30$ and $\pi_\omega = 1/30, \forall \omega \in \Omega$). The scenarios for each random variable that is represented explicitly in the scenario tree are generated from the previous four weeks' data. These scenarios and the four weeks' that are used to generate them are updated as our model rolls forward from $\tau = 1$ to $\tau = 8760$ (or $\tau = 8784$). Using our previous notation, let $\zeta^\tau_{h,d,w}$ denote the historical value of ζ from hour h of day d from w weeks before hour τ, for all $h \in H = \{1,2,\ldots,24\}, d \in D = \{1,2,\ldots,7\}$, and $w \in W = \{1,2,\ldots,4\}$. For all $h \in H$, we let:

$$\overline{\zeta}_h = \frac{\sum_{d \in D, w \in W} \zeta^t_{h,d,w}}{|D| \cdot |W|};$$

denote the sample-average value of ζ that is observed during hour h over the previous four weeks. The values of $\overline{\zeta}_h$ are used as the baseline value of each random variable in the scenario-generation technique. We compute also the average of the sample averages:

$$\overline{\zeta} = \frac{1}{|H|} \overline{\zeta}_h;$$

and the sample variance of ζ:

$$\overline{\sigma}^2 = \frac{\left(\sum_{h,d,w} \zeta^t_{h,d,w} - \overline{\zeta}\right)^2}{|H| \cdot |D| \cdot |W| - 1}.$$

We use two scenario-generation techniques. The first scenario-generation technique, to which we refer as using hourly white noise, generates scenarios by adding a different randomly sampled unbiased Gaussian-distributed white noise with variance equal to $\overline{\sigma}^2$ to $\overline{\zeta}_h, \forall h \in H$. Our second scenario-generation process, to which we refer as using scenario-consistent white noise, generates a scenario by adding the same randomly sampled unbiased Gaussian-distributed white noise with variance equal to $\overline{\sigma}^2$ to $\overline{\zeta}_h, \forall h \in H$. The solar-availability profiles are truncated to be non-negative, as negative solar availability is physically meaningless.

6. Results

6.1. Ideal benchmark

Fig. 2 illustrates the general framework for analyzing our results. It shows the hourly flows of thermal energy during 18–19 July, 2010 of a CSP plant with an SM of 2.0 and six hours of TES that is located in Tonopah, NV. The two sets of bars that are above the horizontal axis indicate the amount of energy that is available to CSP plant during each hour (*i.e.*, *via* the solar field and TES). The set of bars that is below the horizontal axis indicates thermal energy that is converted into electricity by the powerblock. 18 July has the highest load of 2010. As is common on summer days in North America, both 18 and 19 July, 2010 have continuous blocks of time during which the eight highest loads of the days occur. These blocks of time are indicated by the thick blue lines that are at the bottom of Fig. 2.

Both 18 and 19 July have relatively good solar availability, and the

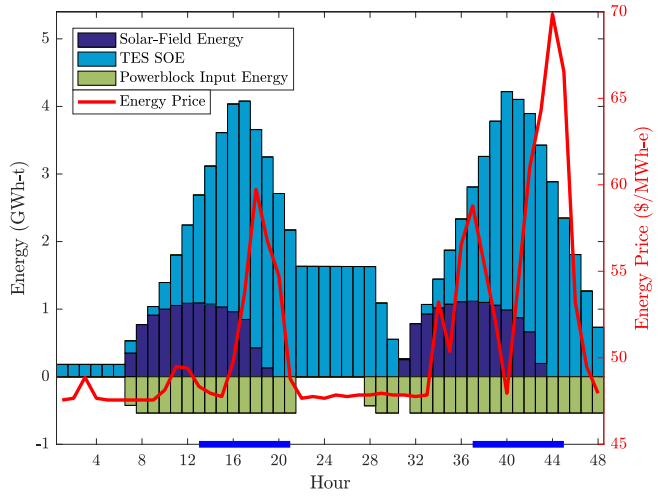

Fig. 2. Hourly thermal energy collected by the solar field, SOE of TES, and powerblock input energy during 18 and 19 July, 2010 of a CSP plant in Tonopah, NV with an SM of 2.0 and six hours of TES and hourly electricity prices. The horizontal blue lines at the bottom of the figure indicate the eight highest-load hours during each of the two days.

CSP plant meets the reliability target fully. Indeed, the CSP plant is operating at its nameplate capacity during the full block of target hours during these two days. Our reliability criterion requires only that the plant have sufficient energy available to operate at its nameplate capacity if system conditions (*e.g.*, a supply shortfall) warrant such a need. Our reliability criterion does not require the plant to operate at its nameplate capacity during the target hours. Nevertheless, the plant operates at its capacity during the target hours because the electricity-price and solar-availability patterns justify doing so.

The TES of the CSP plant reaches its energy-storage capacity at the end of hours 16 and 39. As such, a total of 1.22 GWh-t and 1.67 GWh-t, respectively, of excess thermal energy that is collected by the solar field is curtailed during the two days. This curtailed energy could operate the powerblock at its nameplate capacity for about 2.2 hours and 3.1 hours, respectively. The CSP plant shuts-down immediately after the eight-hour block of highest loads during 18 July. However, the plant remains online after the eight-hour block during 19 July. The plant remains online during the second day because there are higher evening electricity prices compared to those during 18 July. Overall, Fig. 2 shows that during summer days with relatively good solar resource, a CSP plant with an SM of 2.0 and six hours of TES can meet our reliability criterion with minimal or no profit impact.

Fig. 3a summarizes the hourly operation during 1–2 February, 2010 of the same CSP plant that is illustrated in Fig. 2. As is common during winters in North America, the load profile during these two days has morning and afternoon peaks, meaning that the eight highest-load hours of each of the two days occur as two distinct blocks of time during each day. Fig. 3a shows that these two days have relatively poor solar resource. During the two days that are shown in the figure, the solar field delivers only 1.83 GWh-t of energy, which can operate the powerblock at its nameplate capacity for a total of about 3.4 hours. Stored energy that is carried from 31 January in the TES supplements the limited solar energy that is available during these two days. Despite having this stored energy available, the CSP plant is not able to attain the reliability target and has a total energy deficit of about 1.86 GWh-t across the two days (*i.e.*, the plant would need an additional 1.86 GWh-t to meet the reliability target fully during these two days).

Unlike the case that is shown in Fig. 2, the operating profile that is summarized in Fig. 3a is constrained greatly by the reliability criterion. The powerblock is kept online during the target hours, so it is available to operate at its nameplate capacity if necessary. However, with the

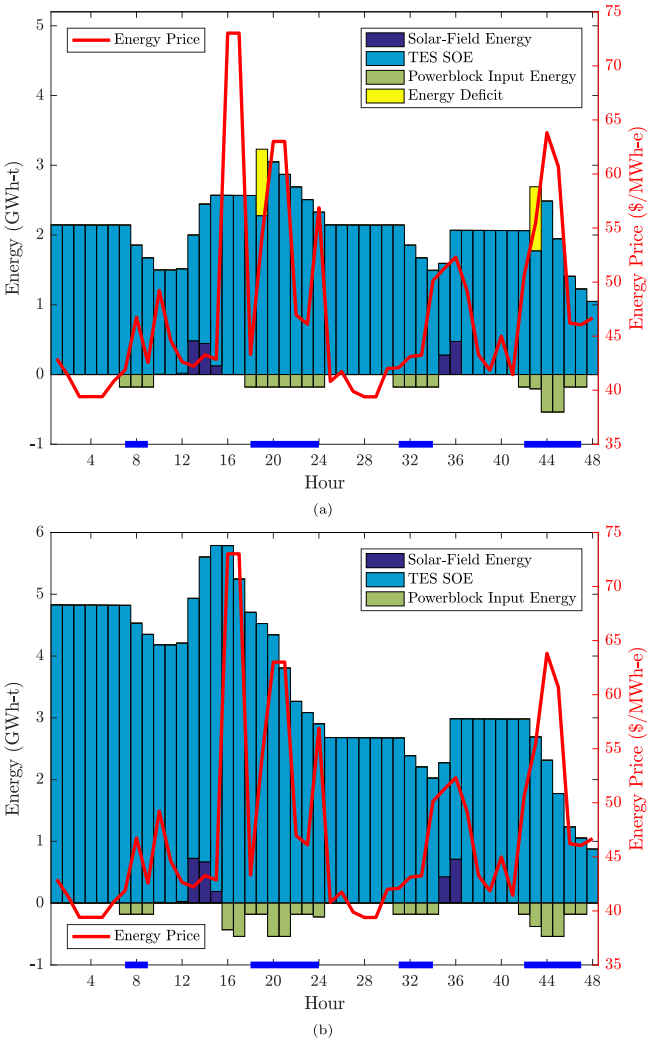

Fig. 3. Hourly thermal energy collected by the solar field, SOE of TES, powerblock input energy, and energy deficit during 1 and 2 February, 2010 of a CSP plant in Tonopah, NV with (3a) an SM of 2.0 and six hours of TES and (3b) an SM of 3.0 and 12 h of TES and hourly electricity prices. The horizontal blue lines at the bottom of the figure indicate the eight highest-load hours during each of the two days. The two energy-deficit bars in Fig. 3a depict the total energy deficit to meet the reliability target during the two corresponding target-hour blocks.

exception of hours 44 and 45, the powerblock is operated at its minimum point. The plant is operated in this manner because energy needs to be retained in the TES to meet the reliability criterion during the full block of target hours. As such, despite electricity prices being relatively high during hours 16,17,19–21, and 24, electric output of the CSP plant is zero or near-zero during these hours.

Fig. 3b summarizes the hourly operation during 1–2 February, 2010 of a CSP plant with an SM of 3.0 and 12 h of TES that is located in Tonopah, NV. Contrasting the two plots in Fig. 3 shows that having a larger configuration has notable operational impacts, which improve the profit and reliability performance of the plant. The higher SM of the larger plant results in more energy being collected by the solar field—a total of 2.77 GWh-t over the two days that are shown, which is sufficient to operate the plant at its nameplate capacity for a total of about 5.2 hours. The larger TES system carries more energy from 31 January, which supplements the increased thermal energy that is gathered and allows the larger plant to meet its reliability target during the days that are shown in Fig. 3b without any energy deficit. To conserve energy, the larger plant does operate at its minimum point during some of the target

hours. However, because it has more energy available than the smaller configuration, the larger plant operates at its nameplate capacity during hours 17,20,21,44, and 45, which allows it to exploit the corresponding high electricity prices.

Despite the improved performance that is illustrated in Fig. 3b (*vis-à-vis* Fig. 3a), a larger CSP plant can experience energy deficits during prolonged periods with poor solar resource. Fig. 4 illustrates energy imbalances during each day of 2010 for CSP plants at Tonopah, NV with the two configurations. The bars below the horizontal axis indicate daily energy deficits in meeting the reliability target (for days during which there is an energy deficit). The bars above the horizontal axis indicate daily thermal-energy curtailments (for days during which there is energy curtailment). The small and large plant configurations experience energy deficits during 165 days and 20 days, respectively, and the solar energy that the plants receive meet 80% and 96% of what is required to meet the reliability target. Energy deficits for the larger plant all occur during the winter, whereas the smaller plant does experience some deficits during the summer. The CSP plants could reduce or eliminate energy deficits if they have the ability to avoid energy curtailment *via* long-duration TES. The smaller plant curtails a total of 200 GWh-t over the year and has a total energy deficit of 203 GWh-t, whereas these values are 300 GWh-t and 30 GWh-t for the larger plant.

The year 2010 has exceptionally poor solar availability. Fig. 5 provides box plots that show the annual energy deficits of CSP plants in Tonopah, NV with the two configurations for different number of days to which the reliability target is applied. The energy deficits are given as percentages of the total energy that is needed to meet the reliability target fully (for the chosen number of days during which it applies). Fig. 5a highlights the fact that a CSP plant with six hours of TES is undersized to meet our reliability criterion in the future when changes in net-load profiles may call upon it to provide energy during days that have relatively low loads today. Even if the TES of such a plant is charged fully, its powerblock can operate at its nameplate capacity for at most six hours (if relying solely on stored energy). As such, the plant *must* have some solar-energy input to meet the eight-hour reliability criterion during a given day. Conversely, so long as the TES system is charged sufficiently, a CSP plant with the larger configuration can meet

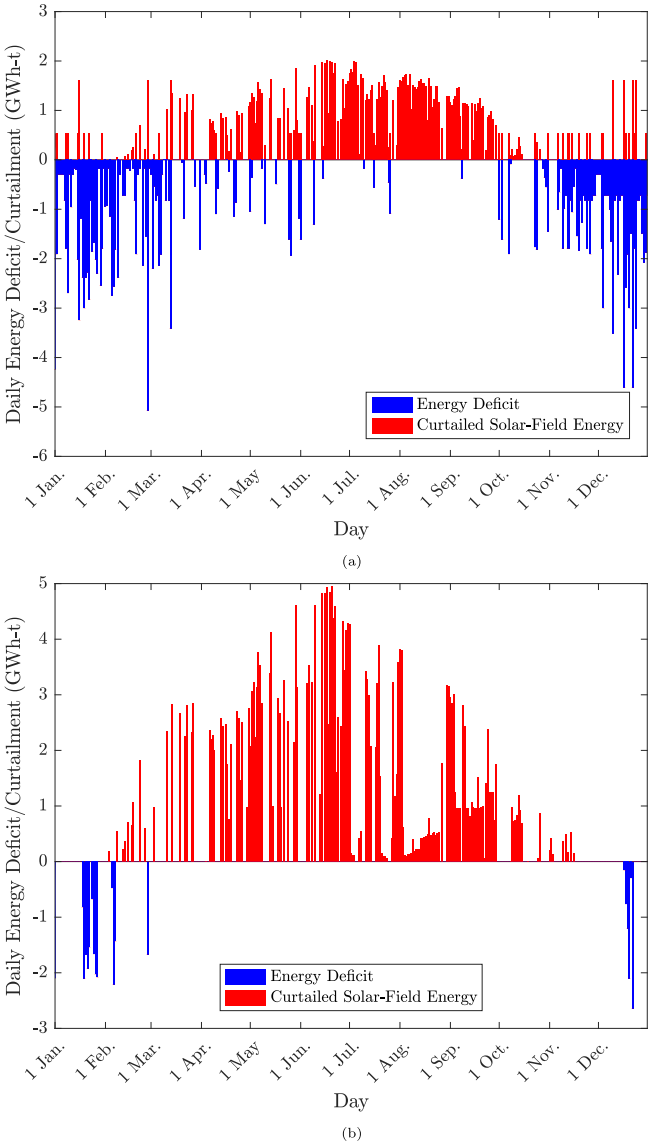

Fig. 4. Energy deficit and curtailed solar-field energy during each day of 2010 for a CSP plant in Tonopah, NV with (4a) an SM of 2.0 and six hours of TES and (4b) an SM of 3.0 and 12 h of TES.

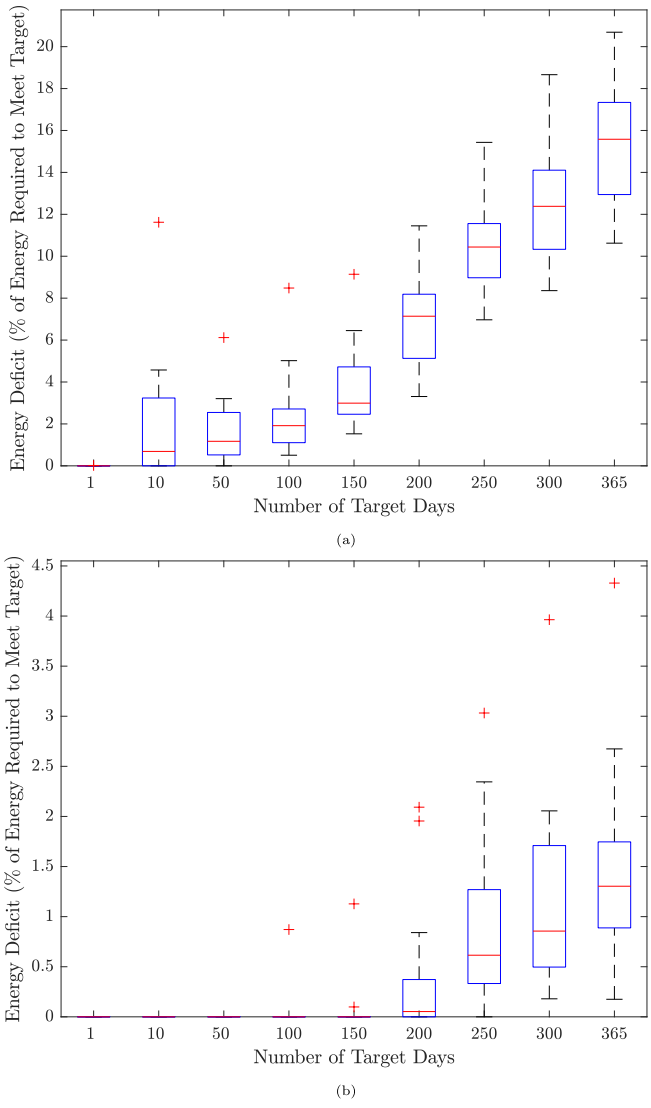

Fig. 5. Standard box plots of total annual energy deficit for a CSP plant in Tonopah, NV with (5a) an SM of 2.0 and six hours of TES and (5b) an SM of 3.0 and 12 h of TES, for different numbers of days to which the target applies. Energy deficits are given as percentages of total energy that is needed to meet the target fully. Each box gives the 25th, 50th, and 75th percentiles. The whiskers represent the range of non-outliers observations, where outliers are defined as being more than 150% of the interquartile range less than the 25th percentile or more than the 75th percentile. Outliers are indicated with '+'.

the reliability criterion during a single day with zero solar availability.

Fig. 5b shows that a properly sized CSP plant can meet a power system's reliability needs fully for the foreseeable future, wherein reliability is determined largely by performance during hot summer days. Even in the distant future when resource-adequacy performance may be measured during other periods of the year, the CSP plant's energy deficit is below 3% during all but one of the years that we study. Tonopah, NV has amongst the highest energy deficits of the locations that we study. Indeed, the 4% energy deficit for the larger plant configuration that is summarized in Fig. 4b is an outlier amongst all of the location/year combinations that we study. These results are due to Tonopah, NV being the most northerly amongst the locations that we consider, which gives rise to many cloudy winter days. These characteristics of the location lead to lower CSP output during many lower-demand days, which gives rise to greater energy deficits if the reliability target applies to more days.

Fig. 6 gives a broader feel for the results of our analysis by showing the range of average annual energy deficits of CSP plants across the locations that we study. The energy deficit for each location is averaged across the years that we examine and reported as a percentage of the energy that is needed to meet the reliability target fully. Rather than plotting the energy deficits for all 27 locations, we show ranges for three clusters of locations that have different annual-average daily DNIs. The figures demonstrate that for the near future, CSP plants with at least six hours of TES can provide very high capacity value throughout the southwestern US, with the energy deficit being less than 4% in most cases. This finding can be explained by Fig. 4, which shows that the energy deficit is low during the summer, which is when load peaks occur currently. Contrasting Fig. 6 with the results of Yagi et al. [10] shows that profit-driven operation of a CSP plant does not impact its reliability contribution in any marked way. This lack of impact is because the operational flexibility that the TES engenders allows the plant to operate 'around' energy-price patterns, so long as it maintains some stored energy to meet the reliability target.

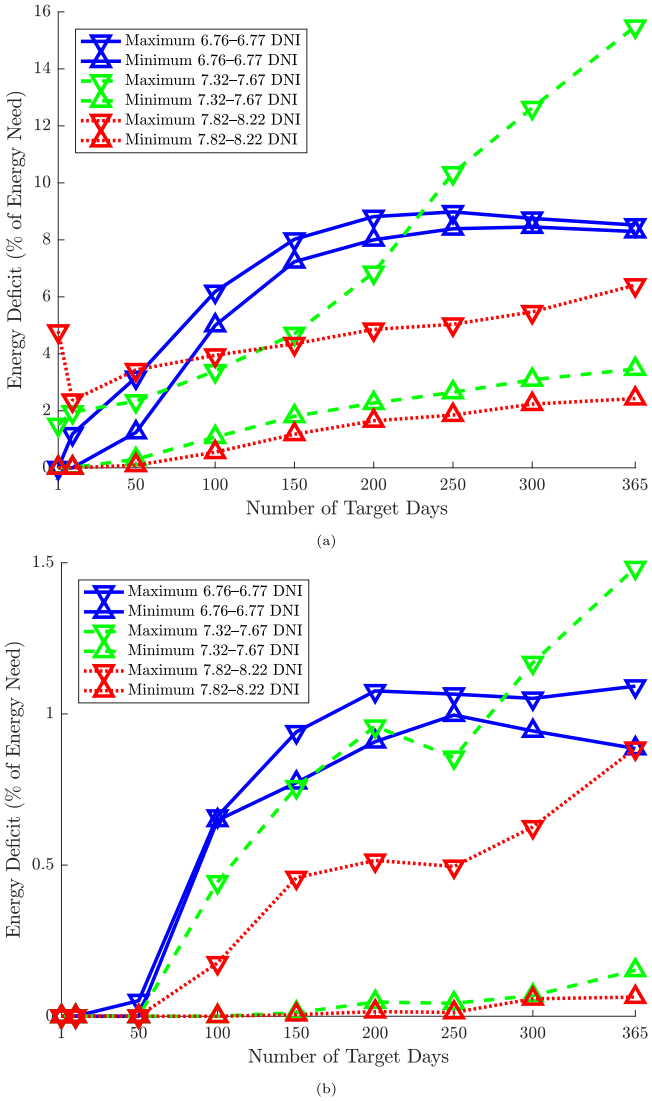

Fig. 6. Ranges across the locations that are studied of average annual energy deficits for CSP plants with (6a) SMs of 2.0 and six hours of TES and (5b) SMs of 3.0 and 12 h of TES, for different numbers of days to which the target applies. Energy deficits are averaged across years for each location and given as percentages of total energy that is needed to meet the target fully. The locations are clustered into three groups, based on annual-average daily DNI.

6.2. *Myopic decisions*

We explore the sensitivity of the results to myopic decisions by examining the performance of a CSP plant in Tonopah, NV with an SM of 3.0 and 12 h of TES. We focus our analysis on the years 2010 and 2011, which yield the greatest and least energy deficits, respectively, in the ideal benchmark. We assume that the reliability target applies to all 365 days of the years, allowing us to assess the robustness of the reliability contribution of a CSP plant in the far future, when net-load patterns may be significantly different than they are today.

Table 3 summarizes the profits and energy deficits of the CSP plant under three behavioral assumptions—the ideal benchmark, myopic decision making, and myopic decision making that neglects the reliability criterion and is concerned solely with maximizing profit. Contrasting this third case with the others allows us to gauge the profit impact of meeting the reliability criterion. The profits that are reported in Table 3 account for the cost of fulfilling the energy deficit using natural gas as a replacement fuel in the CSP plant (*i.e.*, assuming that the plant combusts natural gas as a source of thermal energy). We assume this natural-gas combustion to be 85%-efficient in delivering thermal energy [26]. According to United States Energy Information Administration, the average delivered costs of natural gas for the electricity industry in Nevada were $5.75/MMBTU and $5.00/MMBTU during the two years, respectively. These prices are used in computing the cost of the replacement energy.

Comparing the energy deficits that are reported in Table 3 for the first two cases shows that myopic decisions increases the energy deficits only slightly. Figs. 5 and 6 show that the energy deficits have greater variability as a result of differences between locations and years than Table 3 shows resulting from myopic decision making. Thus, our findings under the ideal benchmark are robust to the operational assumption. Moreover, comparing profits that are earned if the reliability requirement is relaxed to cases in which it is not shows that the reliability criterion impacts CSP profits by less than 1.2%. These results show that CSP plants can serve as economic sources of supply reliability, as meeting the reliability criterion has minimal profit impacts.

Table 3
Profits earned ($ million) and energy deficits to meet the reliability target during all 365 days of 2010 and 2011 (%) for a CSP plant in Tonopah, NV with an SM of 3.0 and 12 h of TES with different levels of operational myopia.

Year		Behavioral Assumption		
		Ideal Benchmark	Myopic	Profit-Only Myopic
2010	Profit	53.03	52.98	53.62
	Deficit	4.05	7.82	n/a
2011	Profit	61.02	61.02	61.24
	Deficit	0.18	2.71	n/a

6.3. Impacts of uncertainty

We analyze the impacts of uncertainty in two steps. We begin by examining day-ahead persistence forecasts using the same paradigm whereby operational decisions are made one hour at a time using a rolling 24-h optimization horizon. We consider a CSP plant in Tonopah, NV with an SM of 3.0 and 12 h of TES during the years 2010 and 2011 and assume that the reliability target applies to all 365 days of the two years.

Table 4 summarizes the profits and energy deficits of the CSP plant using persistence forecasts of all or some of the uncertain data. The profits that are reported account for the cost of fulfilling the energy deficit using replacement natural gas. The first case that is summarized in Table 4 assumes that persistence forecasts are used for all of the uncertain system conditions. Comparing the results in this case to what is reported in Table 3 shows that persistence forecasts yield considerably worse performance, especially with respect to meeting the reliability criterion. The remaining two cases that are summarized in Table 4 use persistence forecasts for all of the uncertain data except for the target hours to which the reliability criterion applies and solar availability, respectively, assuming perfect foresight for these two data sets in the two cases. Contrasting these two cases with the others shows that performance of the CSP plant is relatively similar between using persistence forecasts for all of the uncertain data and assuming perfect foresight of the target hours. On the other hand, having perfect foresight of solar availability improves the operational performance of the CSP plant considerably. This result means that improved forecasting of solar availability (we use very simple persistence forecasts) can improve the performance of a CSP plant considerably whereas improved load forecasting is relatively unimportant.

In addition to persistence forecasts, we explore the use of two-stage stochastic optimization to determine CSP-plant operations one hour at a time using a rolling 24-h optimization horizon. Table 5 summarizes our results of employing stochastic optimization, taking the same case as before of a CSP plant in Tonopah, NV with an SM of 3.0 and 12 h of TES during the years 2010 and 2011 assuming that the reliability target applies to all 365 days of the two years. Table 5 reports for the two scenario-generation techniques that we employ the same metrics that are given in Table 3. Both cases that are reported in Table 5 use day-ahead persistence forecasts for the target hours and scenarios for electricity prices and solar availability.

The results for the two scenario-generation techniques are significantly different. Using hourly white noise provides individual scenarios with variability around the baseline profile. Conversely, using scenario-consistent white noise provides scenarios without this variability. Instead, scenario-consistent white noise produces scenarios that are shifted up or down from the baseline profile based on the single random sample. Given these differences, using hourly white noise yields performance that is similar to using persistence forecasts for *all* of the uncertain data. Indeed, this scenario-generation technique yields similar energy deficits but higher profits compared to using persistence forecasts. Scenario-consistent white noise yields operational behavior that is comparable, in terms of energy deficit, to having perfect foresight of solar availability. However, scenario-consistent white noise yields much lower profits compared to the other cases that we examine. Scenario-consistent white noise performs in this manner because it yields conservative operational behavior. Each scenario that is generated using scenario-consistent white noise has the same random noise applied to the baseline solar-availability level for each hour. As such, some scenarios that are generated (for which the random noise is negative and large in magnitude) predict sustained periods of very low or zero solar availability. These scenarios drive the operational model to keep more energy in the TES, which improves the performance of the plant *vis-à-vis* the reliability criterion. However, this conservative behavior causes the CSP plant to forego profit opportunities, *e.g.*, when prices are high or if future solar conditions are higher than the conservative scenarios predict, resulting in thermal energy being wasted because the combined capacity of the TES and powerblock cannot accommodate it.

Table 4
Profits earned ($ million) and energy deficits to meet the reliability target during all 365 days of 2010 and 2011 (%) for a CSP plant in Tonopah, NV with an SM of 3.0 and 12 h of TES with use of different persistence forecasts.

Year		Persistence Forecasts Used		
		All Data	All Except Target Hours	All Except Solar Availability
2010	Profit	49.57	49.56	52.49
	Deficit	25.03	24.68	10.67
2011	Profit	57.89	58.14	60.68
	Deficit	19.28	18.46	5.11

Table 5
Profits earned ($ million) and energy deficits to meet the reliability target during all 365 days of 2010 and 2011 (%) for a CSP plant in Tonopah, NV with an SM of 3.0 and 12 h of TES with use of two-stage stochastic optimization.

Year		Scenario-Generation Method	
		Hourly White Noise	Scenario-Consistent White Noise
2010	Profit	50.63	44.21
	Deficit	23.50	10.70
2011	Profit	59.31	51.03
	Deficit	19.54	7.66

To illustrate the impacts of using persistence forecasts versus stochastic optimization, Fig. 7 summarizes the hourly operation of a CSP plant at Tonopah, NV with an SM of 3.0 and 12 h of TES during 4–5 January, 2010. Figs. 7a–7c assume myopic hourly decisions, but correspond to cases in which perfect foresight, day-ahead persistence forecasts, and stochastic optimization, respectively, are employed. Fig. 7d summarizes the differences in powerblock input energy between the operational assumptions. Both of 3 and 4 January have relatively good solar resource, meaning that day-ahead persistence forecasts provide relatively good operational decisions for 4 January. Indeed, comparing Figs. 7a and 7b shows that plant operations during 4 January using persistence forecasts are very similar to those that are obtained with perfect foresight. In both of these cases the powerblock is started-up during hour 6 and it continues operating for the remainder of the day while operating the powerblock at its nameplate capacity during high-price hours of 4 January.

Plant operations during 4 January are significantly different when using stochastic optimization (*cf.* Fig. 7c). Because the model includes scenarios with relatively low or zero solar availability, the SOE of TES is kept considerably higher compared to the other two operational profiles. Because 4 January does have relatively high solar availability, the SOE of TES peaks at its limit at the end of hour 14 and the plant increases its electric output between hours 14 and 16 (when electricity prices are relatively low) to avoid curtailing unanticipated solar energy. This overly conservative use of TES gives rise to the poor profit performance when employing scenario-consistent white noise to generate scenarios.

The operation of the CSP plant during 5 January that is illustrated in Fig. 7b demonstrates the pitfall of relying upon persistence forecasts. Using persistence forecasts, the plant is operated during the early morning hours of 5 January expecting relatively good solar availability. As such, the TES is depleted by hour 33 and during hour 43 the CSP plant has an energy deficit.

Fig. 8 shows daily energy deficits during each day of 2010 for a CSP plant in Tonopah, NV with an SM of 3.0 and 12 h of TES under the three operational assumptions that are summarized in Fig. 7. With perfect foresight, energy deficits are limited to the winter. Persistence forecasts

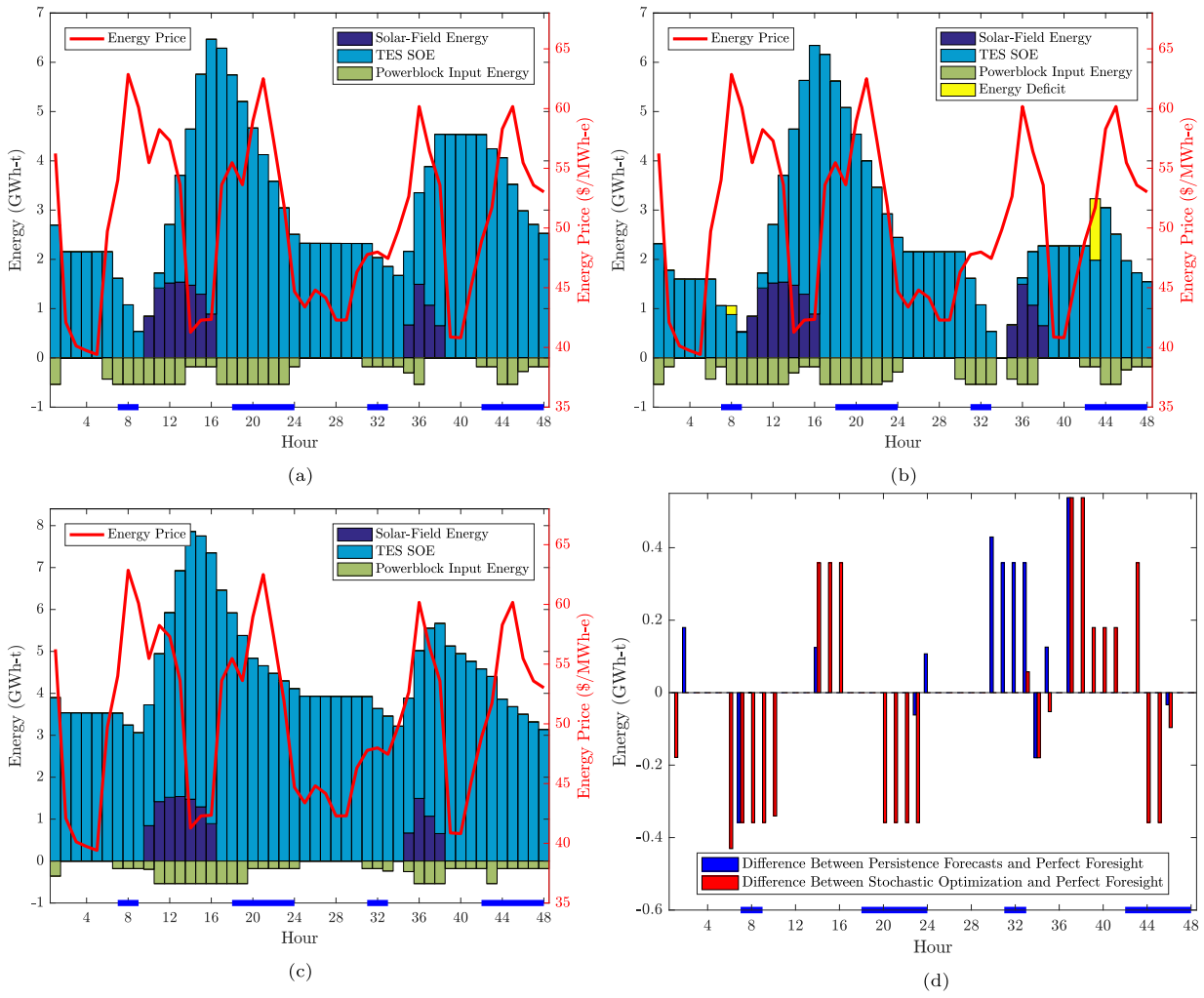

Fig. 7. Hourly thermal energy collected by the solar field, SOE of TES, powerblock input energy, and energy deficit during 4 and 5 January, 2010 of a CSP plant in Tonopah, NV with an SM of 3.0 and 12 h TES and hourly electricity prices, assuming myopic decisions with (7a) perfect foresight, (7b) day-ahead persistence forecasts, and (7c) stochastic optimization using scenario-consistent white noise. Fig. 7d summarizes differences in powerblock input energy between the different operational assumptions. The horizontal blue lines at the bottom of the figure panels indicate the eight highest-load hours during each of the two days. The two energy-deficit bars in Fig. 7b depict the total energy deficit to meet the reliability target during the two corresponding target-hour blocks.

yield considerably more energy deficits, in terms of the number of days during which deficits occur and the magnitude of the deficits. These deficits occur when a day with poor solar availability follows a day with relatively good solar availability. The conservatism of the scenarios that underlie our stochastic optimization reduce considerably (*vis-à-vis* using persistence forecasts) the frequency and magnitude of the energy deficits.

7. Conclusions

This paper studies the potential for CSP plants to serve the reliability needs of power systems. In doing so, we impose a reliability criterion that is robust to changes in net-load patterns that are expected due to the adoption of renewable energy. A key novelty of our work is that we examine the reliability contribution of CSP through the lens of a profit-driven plant owner. In addition, we examine the impacts of data availability and forecasting. The model that we develop could be used to optimize CSP-plant operations based on profit and reliability-contribution criteria. We show that during the near future and absent myopic decision making and uncertainty, CSP plants with an SM of 2.0 and six hours of TES can serve reliability needs. Further into the future, when CSP supply may be needed during days with relatively low loads today, a larger plant configuration is necessary to maintain the same level of reliability contribution. These reliability benefits of CSP come with very little profit impact compared to a case in which the plants are operated solely to maximize profit. The limited profit impact stems from the CSP plants leveraging the flexibility that TES provides. We do not require the plants to operate at nameplate capacity during target hours. Rather, we require only that the plants have sufficient energy available to operate at nameplate capacity if doing so is required for purposes of power-system reliability.

We relax the strong assumption of perfect foresight and examine myopic decisions. Conducting these computations one hour at a time is computationally expensive. As such, we focus this analysis on a single location that has relatively poor solar availability and the years with the greatest and least energy deficits. We show that myopic decisions have relatively muted impacts on the profit and reliability contribution of CSP plants. This result is due to TES being used primarily to move energy within or between subsequent days. Such a use of TES can be captured by a 24-h optimization horizon. On rare occasion (*e.g.*, a number of consecutive days with poor solar availability) TES might be used for shifting energy over a longer period of time, which a 24-h optimization horizon cannot capture. Such use of TES is relatively rare, which is why the energy-deficits and profits that are reported in Table 3 are quite similar with and without myopic decisions.

We examine the impacts of uncertainty in two ways. Through the use

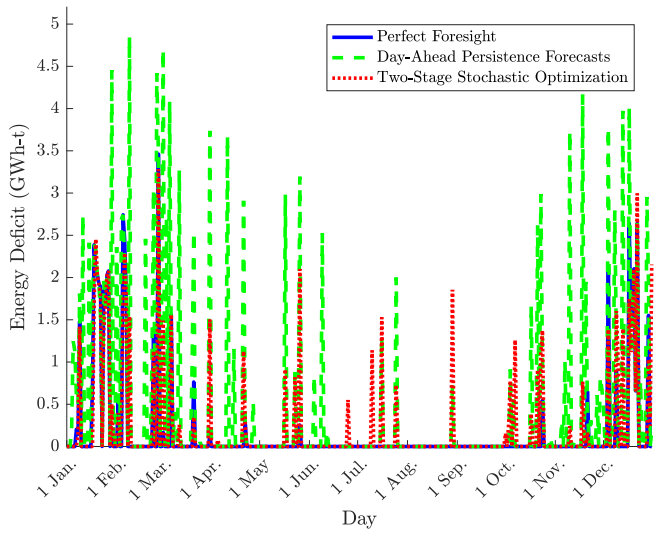

Fig. 8. Energy deficit during each day of 2010 for a CSP plant in Tonopah, NV with an SM of 3.0 and 12 h of TES assuming hourly plant operations with perfect foresight, day-ahead persistence forecasts, or stochastic optimization with scenario-consistent white noise.

of persistence forecasts we demonstrate that predicting future solar availability (24 h into the future) is key in attaining good reliability and profit performance. Forecasting target hours is less important because, so long as it has sufficient stored energy, the TES provides the plant with operational flexibility to produce during most any eight-hour block of time. Having an accurate solar-availability forecast is key, however, in ensuring that TES has sufficient stored energy. We examine a very simple scenario-generation technique, which can be used within a stochastic-optimization framework to deliver reliability performance that is comparable to having perfect foresight of solar availability. This reliability performance comes at a profit cost, due to the resultant conservative operation of the plant. An alternative scenario-generation technique that we examine yields profits that are comparable to having perfect foresight of uncertain system conditions, but worse reliability performance.

How a CSP-plant owner trades-off between profits from energy sales and reliability performance is, in part, a matter of the design of the underlying market in which the plant participates. Some markets include explicit auctions that remunerate resources for providing reliable supply capacity. Cramton and Stoft [27] provide a formative proposal for designing such market mechanisms. Finon and Pignon [28] provide a retrospective view on the early designs of these markets. Keppler [29] justifies the use of an explicit capacity mechanism to address security-of-supply externalities and asymmetric incentives for capacity investment. Duggan [30] provides a survey of the capacity-mechanism literature. Other markets rely upon scarcity pricing—electricity prices having extreme spikes when the power system experiences a capacity shortfall—to incentivize the provision of supply. Hogan [31] provides a succinct vision of this market design, especially in a future with high penetrations of low-marginal-cost resources. Oren [32] proposes the design of a scarcity-pricing mechanism that uses call options to hedge against price volatility. Imran and Kockar [33] provide a technical comparison of the designs of electricity markets in North America and Europe, including mechanisms for ensuring the availability of adequate generating capacity. Should a CSP plant participate in a market with an explicit capacity mechanism, the relative profits that are earned from the provision of capacity and energy would play a key role in determining the conservatism of the plant's operation *vis-à-vis* its reliability contribution.

The plant-performance metrics that we report from using stochastic optimization and persistence forecasts represent a worst-case scenario, because we use very simple forecasting and operational techniques. The use of more sophisticated techniques can improve CSP performance with respect to reliability contribution and profit. We demonstrate that improving day-ahead solar-availability forecasting will have the most pronounced impact on improving plant operations. A number of more sophisticated forecasting techniques, including approaches based on satellite imagery [34], time-series models [35], and ensemble methods [36], are proposed in the literature and should yield much better performance than our simulations provide. We do not explore such techniques, as our research focus is not on developing solar-availability forecasts. However, surveys that examine the performance of forecasting methods are in the literature [37]. A comprehensive analysis of the impacts of improved solar-availability forecasts *vis-à-vis* our findings would be a fruitful avenue for future work.

Our analysis assumes that the CSP plant relies solely upon solar thermal energy to produce electricity and that energy deficits are fulfilled using natural gas. However there are alternative pathways that could maintain high reliability contribution without the use of natural gas. For instance, inductive or resistive heaters could be installed in the TES system of a CSP plant. Such heaters could be used to store excess power-system energy (*e.g.*, from solar photovoltaic and wind generators), which would supplement solar-field energy. Converting electricity into thermal energy is nearly 100%-efficient. However, the roundtrip efficiency of this process would be lower, because the stored thermal energy would be converted back into electricity through a Rankine cycle. Nonetheless, there may be considerable periods of time in a system with high renewable-energy penetrations during which the system has excess electricity. Indeed, Fig. 4 shows that the CSP plants experience thermal-energy curtailment that is on-par with or exceeds greatly the plants' energy deficits in meeting the reliability target. These findings point to the transformational benefits that a scalable and economic seasonal-energy-storage technology would have to achieve extremely aggressive decarbonization targets. Incorporating inductive or resistive heaters into CSP plants could help to bridge this current technical gap, reduce energy curtailment, improve CSP-plant performance, and reduce the need for accurate solar-availability forecasting. Alternatively, the CSP plant could utilize renewably-derived fuels, such as synthetic methane or biofuels, to fulfill the small energy deficit. The relative merits of these approaches to supplementing solar thermal energy needs further examination.

CRediT authorship contribution statement

Kenjiro Yagi: Conceptualization, Methodology, Software, Validation, Formal analysis, Investigation, Data curation, Writing, Visualization. **Ramteen Sioshansi:** Conceptualization, Methodology, Resources, Writing, Visualization, Supervision, Project administration, Funding acquisition. **Paul Denholm:** Conceptualization, Methodology, Resources, Writing, Visualization, Supervision, Project administration, Funding acquisition.

Declaration of Competing Interest

The authors declare that they have no known competing financial interests or personal relationships that could have appeared to influence the work reported in this paper.

Acknowledgments

This work is authored, in part, by National Renewable Energy Laboratory, which is operated by Alliance for Sustainable Energy, LLC, for United States Department of Energy (DOE) under contract number DE-AC36-08GO28308. Funding is provided by DOE's Office of Energy Efficiency and Renewable Energy Solar Energy Technologies Office. The views expressed in the article do not represent necessarily the views of DOE or the US government. The US government retains and the

publisher, by accepting the article for publication, acknowledges that the US government retains a nonexclusive, paid-up, irrevocable, worldwide license to publish or reproduce the published form of this work, or allow others to do so, for government purposes. The authors thank Mark Mehos, Craig Turchi, Jeffrey Logan, Aaron Bloom, Armin Sorooshian, the editors, and three reviewers for helpful discussions, comments, and suggestions. Billy Roberts provided invaluable assistance in developing Fig. 1. The material in this paper is based upon work that is supported financially by Alliance for Sustainable Energy, LLC through subcontract XEJ-7-70018-01. The first author thanks Tokushu Tokai Paper Co., Ltd. for its financial support for his Ph.D. studies at The Ohio State University. Any opinions and conclusions that are expressed in this paper are solely those of the authors. Any remaining errors are entirely those of the authors.

References

[1] Lilliestam J, Labordena M, Patt A, Pfenninger S. Empirically observed learning rates for concentrating solar power and their responses to regime change. Nature Energy 2017;2:1–6.
[2] Pfenninger S, Gauché P, Lilliestam J, Damerau K, Wagner F, Patt A. Potential for concentrating solar power to provide baseload and dispatchable power. Nature Climate Change 2014;4:689–92.
[3] Denholm P, Ela E, Kirby B, Milligan MR. The Role of Energy Storage with Renewable Electricity Generation, Tech. Rep. NREL/TP-6A2-47187, National Renewable Energy Laboratory, Golden, CO (January 2010).
[4] Sioshansi R, Denholm P, Arteaga J, Awara S, Bhattacharjee S, Botterud A, Cole W, Cortés A, de Queiroz A, DeCarolis J, Ding Z, DiOrio N, Dvorkin Y, Helman U, Johnson JX, Konstantelos I, Mai T, Pandžić H, Sodano D, Stephen G, Svoboda A, Zareipour H, Zhang Z. Energy-Storage Modeling: State-of-the-Art and Future Research Directions, IEEE Transactions on Power Systems, In press.
[5] Usaola J. Capacity credit of concentrating solar power. IET Renewable Power Generation 2013;7:680–8.
[6] Akbari-Dibavar A, Mohammadi-Ivatloo B, Zare K, Khalili T, Bidram A. Economic-Emission Dispatch Problem in Power Systems With Carbon Capture Power Plants. IEEE Trans Ind Appl 2021;57:3341–51.
[7] Madaeni SH, Sioshansi R, Denholm P. Estimating the Capacity Value of Concentrating Solar Power Plants: A Case Study of the Southwestern United States. IEEE Trans. Power Systems 2012;27:1116–24.
[8] Madaeni SH, Sioshansi R, Denholm P. Estimating the Capacity Value of Concentrating Solar Power Plants with Thermal Energy Storage: A Case Study of the Southwestern United States. IEEE Trans Power Systems 2013;28:1205–15.
[9] Madaeni SH, Sioshansi R, Denholm P. How Thermal Energy Storage Enhances the Economic Viability of Concentrating Solar Power. Proc IEEE 2012;100:335–47.
[10] Yagi K, Sioshansi R, Denholm P. Evaluating a Concentrating Solar Power Plant as an Extended-Duration Peaking Resource Solar Energy. Solar Energy 2019;191:686–96.
[11] Graves F, Jenkin T, Murphy D. Opportunities for Electricity Storage in Deregulating Markets. Electricity J 1999;12:46–56.
[12] Sioshansi R, Denholm P, Jenkin T, Weiss J. Estimating the Value of Electricity Storage in PJM: Arbitrage and Some Welfare Effects. Energy Econ 2009;31:269–77.
[13] Akbarzadeh S, Valipour MS. Heat transfer enhancement in parabolic trough collectors: A comprehensive review. Renewable Sustainable Energy Rev 2018;92:198–218.
[14] Baharoon DA, Rahman HA, Omar WZW, Fadhl SO. Historical development of concentrating solar power technologies to generate clean electricity efficiently — A review. Renewable Sustainable Energy Rev 2015;41:996–1027.
[15] Mehos M, Turchi C, Jorgenson J, Denholm P, Ho C, Armijo K. Advancing Concentrating Solar Power Technology, Performance, and Dispatchability, Tech. Rep. NREL/TP-5500-65688, National Renewable Energy Laboratory, Golden, CO (May 2016).
[16] Sioshansi R, Denholm P. The Value of Concentrating Solar Power and Thermal Energy Storage. IEEE Trans Sustainable Energy 2010;1:173–83.
[17] Blair N, DiOrio N, Freeman J, Gilman P, Janzou S, Neises T, Wagner M. System Advisor Model (SAM) General Description (Version 2017.9.5), Tech. Rep. NREL/TP-6A20-70414, National Renewable Energy Laboratory, Golden, CO (May 2018).
[18] Sioshansi R, Denholm P. Benefits of Colocating Concentrating Solar Power and Wind. IEEE Trans Sustainable Energy 2013;4:877–85.
[19] Birge JR, Louveaux F. Introduction to Stochastic Programming. corrected Edition. New York, New York: Springer Verlag; 1997.
[20] Martinek J, Jorgenson J, Mehos M, Denholm P. A comparison of price-taker and production cost models for determining system value, revenue, and scheduling of concentrating solar power plants. Appl Energy 2018;231:854–65.
[21] Sengupta M, Habte A, Gotseff P, Weekley A, Lopez A, Anderberg M, Molling C, Heidinger A. A Physics-Based GOES Product for Use in NREL's National Solar Radiation Database, Tech. Rep. NREL/CP-5D00-62776, National Renewable Energy Laboratory, Golden, CO (September 2014).
[22] Sengupta M, Habte A, Gotseff P, Weekley A, Lopez A, Molling C, Heidinger A. A Physics-Based GOES Satellite Product for Use in NREL's National Solar Radiation Database, Tech. Rep. NREL/CP-5D00-62237, National Renewable Energy Laboratory, Golden, CO (July 2014).
[23] Sengupta M, Xie Y, Lopez A, Habte A, Maclaurin G, Shelby J. The National Solar Radiation Data Base (NSRDB). Renewable Sustainable Energy Rev 2018;89:51–60.
[24] Wilcox SM, National Solar Radiation Database 1991-2010 Update: User's Manual, Tech. Rep. NREL/TP-5500-54824, National Renewable Energy Laboratory, Golden, CO (August 2012).
[25] Wagner MJ, Newman AM, Hamilton WT, Braun RJ. Optimized dispatch in a first-principles concentrating solar power production model. Appl Energy 2017;203:959–71.
[26] Peterseim JH, Viscuso L, Hellwig U, McIntyre P. Large capacity, multi-fuel, and high temperature working fluid heaters to optimize CSP plant cost, complexity and annual generation. In: Rajpaul V, Richter C, editors. AIP Conference Proceedings, Vol. 1734. Cape Town, South Africa: American Institute of Physics; 2016.
[27] Cramton P, Stoft S. A Capacity Market that Makes Sense. Electricity J 2005;18:43–54.
[28] Finon D, Pignon V. Capacity mechanisms in imperfect electricity markets. Utilities Policy 2008;16:141–2.
[29] Keppler JH. Rationales for capacity remuneration mechanisms: Security of supply externalities and asymmetric investment incentives. Energy Policy 2017;105:562–70.
[30] Duggan Jr JE. Capacity Market Mechanism Analyses: A Literature Review. Current Sustainable/Renewable Energy Reports 2020;7:186–92.
[31] Hogan WW. Market Design Practices: Which Ones Are Best? IEEE Power Energy Magazine 2019;17:100–4.
[32] Oren SS. Generation Adequacy via Call Options Obligations: Safe Passage to the Promised Land. Electricity J 2005;18:28–42.
[33] Imran K, Kockar I. A technical comparison of wholesale electricity markets in North America and Europe. Electric Power Systems Res 2014;108:59–67.
[34] Alonso-Montesinos J, Batlles FJ. Solar radiation forecasting in the short- and medium-term under all sky conditions. Energy 2015;83:387–93.
[35] Liu Y, Roberts MC, Sioshansi R. A Vector Autoregression Weather Model for Electricity Supply and Demand Modeling. J Modern Power Syst Clean Energy 2018;6:763–76.
[36] Zhang X, Li Y, Lu S, Hamann HF, Hodge B-M, Lehman B. A Solar Time Based Analog Ensemble Method for Regional Solar Power Forecasting. IEEE Trans Sustainable Energy 2019;10:268–79.
[37] Widén J, Carpman N, Castellucci V, Lingfors D, Olauson J, Remouit F, Bergkvist M, Grabbe M, Waters R. Variability assessment and forecasting of renewables: A review for solar, wind, wave and tidal resources. Renewable Sustainable Energy Reviews 2015;44:356–75.